AIAA JOURNAL
Vol. 36, No. 1, January 1998

Development of a Global Interferometer Skin-Friction Meter

T. J. Garrison* and M. Ackman†
Louisiana State University, Baton Rouge, Louisiana 70803

An improved method for measuring skin friction in two-dimensional flows is described. The instrument, termed a global interferometer skin-friction meter, is used to measure the shape of a thin oil film placed on a test model subject to aerodynamic shear. The oil film shape is then related to the applied shear through lubrication theory. Through acquisition of a single image of the oil film interference pattern, the skin-friction distribution can be obtained at any point covered by the film. Enhancements to the method are presented that may extend the instrument's application to fully three-dimensional flows with time-variant model temperatures. Results from tests performed on flat plate boundary layers along with numerical simulations show the instrument can accurately measure wall shear over relatively large areas in a single test. Results show the method provides numerous advantages over other shear measurement techniques. The instrument's configuration, the theoretical background, and the parameters that influence its accuracy are presented.

Introduction

ACCURATE measurement of the wall shear stress distribution is important for understanding many types of flowfields. Such data are crucial to understanding aerodynamic drag and for evaluating the performance of proposed drag reduction strategies. Moreover, skin-friction data are extremely valuable for validation of computational solutions due to the direct link between the predicted shear stress and the turbulence model. However, despite the importance of accurate skin-friction data, obtaining such, either experimentally or computationally, can be extremely difficult, costly, and time consuming. The level of difficulty increases considerably for measurements in complex, three-dimensional flows with separation.

The primary difficulty with measuring wall shear lies in the lack of a universal measurement technique that can provide accurate data in a wide range of flows. Winter[1] provides a good review of the various wall shear measurement techniques. Nearly all of the existing methods for wall shear measurements, e.g., Preston tubes, Stanton tubes, sublayer fences, electrochemical techniques, and floating element balances, have very limited ranges of application. In general, these methods are intrusive, are restricted to certain types of flows, are limited to flows with modest pressure gradients, and require detailed calibration. Additionally, these methods provide only pointwise data and can be time consuming to implement on large surfaces.

A more recent method of shear measurement that has shown promise is the laser interferometer skin-friction (LISF) meter. The LISF meter was originally invented by Tanner and Blows[2] for use in low-speed flows. The basic principle of operation of the LISF meter is to optically measure the time rate of thinning of an oil film placed on a test surface subject to aerodynamic shear. The rate of thinning of the oil film is determined using optical interference and can be related to the applied shear through lubrication theory.

Although the LISF meter was originally used for low-speed airflows, further development of the method[3–6] has resulted in an instrument that is capable of measurements over a broad range of flow conditions, including supersonic flows,[7–12] shock-wave/boundary-layer interactions with strong pressure gradients and flow separation,[9–12] and more recently two-phase (air-water) and single-phase (water) pipe flows.[13]

Despite its relatively broad range of applicability, the LISF technique suffers from several shortcomings. Foremost, the method provides only pointwise data. Hence, measuring shear distributions over large surfaces is time consuming and may be impractical in some instances. Also, the LISF technique requires that the oil film thickness be recorded continuously during the test run. This can be a significant problem in high-speed flows for which surface waves form on the oil film. These surface waves distort the laser beam that is used to record the time-variant oil thickness and greatly reduce the usable signal. Additionally, in both low- and high-speed flows, dust, vibration, and other effects can create noise that limits the usable signal or renders it useless. Finally, the LISF method requires continuous optical access.

Recently, several groups have developed modified forms of the LISF technique designed to overcome many of the aforementioned limitations. Most notably, these groups have modified the method to provide shear data over either global regions or along lines rather than at discrete points. [To distinguish these instruments from the pointwise LISF instrument, they are referred to herein as global interferometer skin-friction (GISF) meters.] One version of the GISF meter was developed by a group of Russian researchers.[14–16] An advantage of their method is that it accounts for wall shear variations in both the streamwise and spanwise direction and can be used for three-dimensional flows. The primary drawback with their GISF method is that it still requires that data be collected continuously throughout the test run. Hence, it requires continuous optical access and suffers from the problems of surface waves, contamination, and vibration. A similar version of the instrument is reported in Refs. 17 and 18.

An alternate development of a GISF instrument was performed by researchers at NASA Ames Research Center.[19,20] In addition to acquiring shear stress data over global regions in a single test, their version of the GISF method requires acquisition of only a single image of the oil film interference pattern. Hence, the data acquisition and optical access requirements are greatly simplified. In the initial development of the NASA GISF instrument, the method yielded only relative C_f values, and an alternate measurement method, e.g., a Preston tube, was required to determine the reference skin-friction value.[19] Subsequent developments have eliminated the need for a separate measurement of a reference shear, and the method now yields the absolute skin friction. However, unlike the Russian version, the theory behind the NASA method assumes that the shear stress is constant in the flow direction. Hence, the current version of this method is not well suited for application in three-dimensional flows. Effectively, this method provides shear data along a line rather than over a global area.

The primary goal of this paper is to build upon the success of these previous investigations by combining the advantages of both techniques. In particular, this paper focuses on expanding the theoretical framework for the GISF instrument initially developed at NASA to facilitate its application in flows with nonuniform wall shear stress in both the streamwise and spanwise directions. This paper also attempts to quantify the overall uncertainty of the GISF method as

Received Aug. 24, 1996; revision received June 26, 1997; accepted for publication Aug. 11, 1997.

*Assistant Professor, Department of Mechanical Engineering. Member AIAA.
†Research Assistant, Department of Mechanical Engineering. Student Member AIAA.

well as the influence of the various operational parameters associated with the technique. The ultimate objective is to develop a wall shear measurement technique that will work in a broad range of flows, provide accurate data over relatively large surfaces in a single test, require no calibration, and be simple and cost effective to implement.

Description of Experiments

Wind-Tunnel Facility

The experiments were performed in the subsonic wind-tunnel facility at Louisiana State University. The tunnel consists of a 12:1 contraction with honeycomb and screens, a test section, a diffuser, and a variable pitch fan. The test section is 2.4 m long with a rectangular cross section that is 0.46 × 0.6 m. A 3.3-m-long 2.6:1 diffuser section leads to an axial fan capable of delivering 30,000 ft^3/min. The pitch of the fan blades is adjustable, providing a test section velocity range from 10 to 57 m/s. The turbulence level is between 2 and 3% over a majority of the velocity range but increases rapidly to over 6% at the lowest operating velocity.

A flat plate model was used to produce the results presented in this paper. It is constructed of 1.0-cm-thick acrylic sheet and is 0.94 m long and 0.41 m wide with a sharp leading edge. The model is mounted in the freestream flow, and its angle of attack can be adjusted to align it with the freestream flow direction. The alignment was carried out by balancing static pressure taps along the length of the flat plate to ensure a zero pressure gradient, i.e., flat plate conditions. The plate was adjusted until the pressure gradient was less than 4.1 Pa/m. A series of thermocouples were also mounted in the model to record the model surface temperature. This information is needed to accurately determine the oil film viscosity.

Additional shear measurements were made using a Preston tube with the universal calibration developed by Head and Ram.[21] This calibration has a quoted accuracy of 11% where the ratio of the tube diameter to the boundary-layer thickness is much less than 0.1.[22] The Preston tube was constructed from 32-gauge stainless steel tubing (Ø 0.24 mm). Static pressure taps (Ø 2 mm) were installed in the flat plate at the Preston tube measurement locations.

GISF Technique

Experimental Setup

The GISF meter operates on the principle of thin film interference. Referring to Fig. 1, when a monochromatic light source is incident on the surface of a thin film, a portion of the light reflects off the film surface and the remainder passes through this surface and reflects off the fluid-solid boundary. Because of differences in their optical path length, these two reflections will interfere with one another either constructively or destructively. Therefore, a film with varying thickness will produce an interference pattern consisting of alternating areas of constructive and destructive interference. The GISF meter uses such interference patterns to extract the skin-friction distribution over the portion of the model surface coated with the thin film.

Figure 1 shows a schematic of the GISF instrument used in the present study. For the configuration shown, oil is applied on the portion of the model surface over which the shear stress is desired. In practice the oil is applied along discrete lines that then spread into thin film patches during startup of the external flow. The oils used in the present study are Dow 200 Series silicone oils. If the test model surface is not reflective, self-adhesive Mylar® film may be applied to the surface before application of the oil.[12] This material

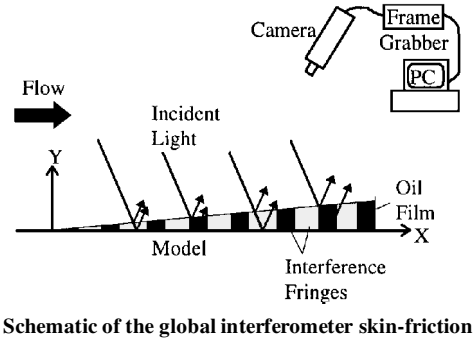

Fig. 1 Schematic of the global interferometer skin-friction meter.

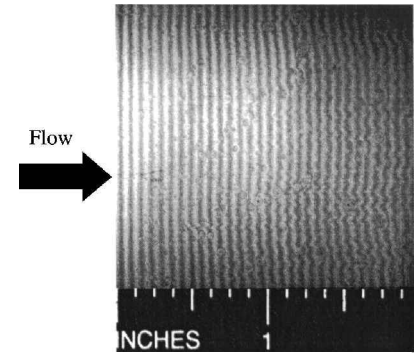

Fig. 2 Sample image of an oil film interference pattern taken on a flat plate with U_∞ = 25 m/s.

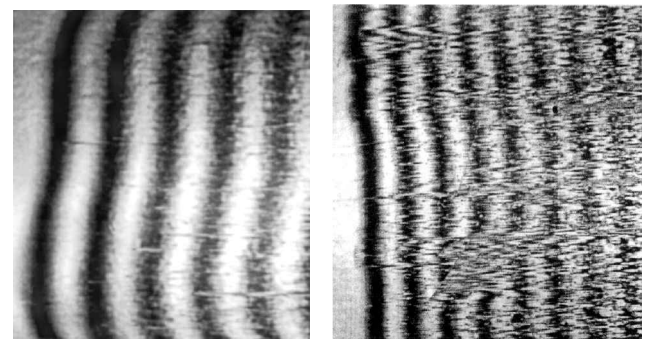

Typical pattern **Heavily contaminated pattern**

Fig. 3 Sample interference patterns illustrating dust contamination.

can be purchased at hobby shops and helps facilitate the use of the GISF technique on nearly any surface.

After startup of the external flow, the oil is thinned due to the applied aerodynamic shear stress. As will be shown in the following section, at any instant in time the local slope of the oil film is directly related to the locally applied shear stress. To record the thin film interference pattern, a charge-coupled device (CCD) camera (640 × 480) is focused on the surface of the oil film (including the leading edge), which is illuminated with a monochromatic light source. A white light can also be used provided an optical bandpass filter is placed over the camera lens to create a single-wavelength fringe pattern. After a designated time period, an image of the oil film interference pattern is digitized by a computer. A sample interference pattern taken on the flat plate model is shown in Fig. 2. The digitized image is then analyzed using the algorithm described in the following section to extract the skin-friction distribution.

Before proceeding with the data analysis procedure, it is important to point out the numerous benefits provided by the configuration shown in Fig. 1. First, the equipment and setup required for the GISF instrument are both simple and inexpensive. Second, because the method is capable of obtaining data over a relatively large area in a single test run, the time required to collect results is significantly less than that needed to obtain data with the various single point methods discussed earlier. Third, as will be shown later, the image of the oil interference pattern need not be acquired during the test run. If optical access is limited, the model can be removed and the pattern recorded elsewhere. Fourth, because continuous data collection is not required, the GISF meter is insensitive to surface waves, vibrations, and surface contaminants. Figure 3 compares a typical image with an image that is highly contaminated with small dust particles. The contamination can be attributed to the cleanliness of the wind-tunnel facility itself, which, for the present tests, is located in a relatively dirty environment. Even though the dust makes extracting the shear at certain points on the film impossible, there is still a substantial region over which the shear can be determined. Moreover, for tunnels operated in cleaner environments and/or by using a filter upstream of the intake, the dust contamination can be minimized. Finally, because the GISF instrument measures the shear stress directly, no calibration is required.

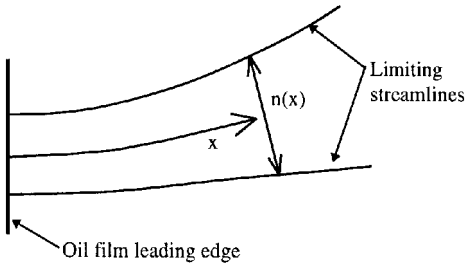

Fig. 4 Coordinate notation.

Data Reduction Algorithm

In developing the original LISF technique, Tanner and Blows[2] and Tanner and Kulkarni[4] showed that the thickness of an oil film placed on a test surface subject to aerodynamic shear could be expressed as

$$h(x,t) = \left[\frac{1}{\sqrt{\tau n}}\int_0^x \left(\frac{n}{\tau}\right)^{\frac{1}{2}} \mathrm{d}x\right] \Big/ \int_0^t \frac{\mathrm{d}t}{\mu_0} \tag{1}$$

Referring to the coordinate system shown in Fig. 4, Eq. (1) shows that the local oil film thickness h depends on the applied shear $\tau(x)$, the local spacing between the limiting wall streamlines, $n(x)$, and the oil viscosity μ_0. This expression holds for flows in which the wall shear varies along the local flow direction and with time-variant temperatures. Equation (1) does assume that the wall shear is not time variant and that the oil temperature, i.e., the model temperature, does not vary spatially.

If one further assumes that the flow is two dimensional, that the temperature is constant, and that the shear stress variation in the flow direction is negligible, Eq. (1) simplifies to

$$h(x,t) = (x\mu_0)/(\tau t) \tag{2}$$

In practice, the assumption that $\tau \neq f(x)$ can be made for flows in which the shear does vary in the streamwise direction, provided all data are collected for very small x values, i.e., data are only collected very close to the leading edge of the oil and τ is approximated as the average shear over this small distance. In the analysis that follows, no assumptions are imposed on Eq. (1) to develop a more general equation that is valid for fully three-dimensional flows and that leads to a true global instrument.

Because it is not possible to solve Eq. (1) explicitly for τ, an iterative approach can be used. This is achieved by taking the shear stress in the denominator outside the integral on the right-hand side of Eq. (1) as an updated value and the shear stress inside the integral from the previous iteration. The iterative form of the equation is shown next:

$$h(x,t) = \left[\frac{1}{\sqrt{\tau_{i+1} n}}\int_0^x \left(\frac{n}{\tau_i}\right)^{\frac{1}{2}} \mathrm{d}x\right] \Big/ \int_0^t \frac{\mathrm{d}t}{\mu_0} \tag{3}$$

Solving this equation for the updated shear stress gives the following iterative equation:

$$\tau_{i+1}(x) = \left(\left\{\int_0^x \left[\frac{n(x)}{\tau_i(x)}\right]^{\frac{1}{2}} \mathrm{d}x\right\} \Big/ \left[h(x)\sqrt{n(x)}\int_0^t \frac{\mathrm{d}t}{\mu_0}\right]\right)^2 \tag{4}$$

Application of Eq. (4) is carried out as follows. The oil film thickness $h(x)$ is determined directly from the interference pattern such as that shown in Fig. 2. This is done by taking a series of cuts through the image along the surface flow direction. The intensity variation along each cut is then plotted and the peaks detected. The peaks are detected using a three-point weighted averaging technique for data smoothing to locate changes in the slope of the signal from positive to negative or vice versa. Figure 5 shows the intensity variation along a cut through the image shown in Fig. 2. Once the peaks are detected, their distance from the oil leading edge can be measured. If the illumination source in Fig. 1 is nearly normal to the plate, each successive peak corresponds to an oil thickness change of $\lambda/4n$, where λ is the wavelength of the incident light source and n is the oil's index of refraction. Knowing this and the peak locations, $h(x)$ can be evaluated at all points on the film.

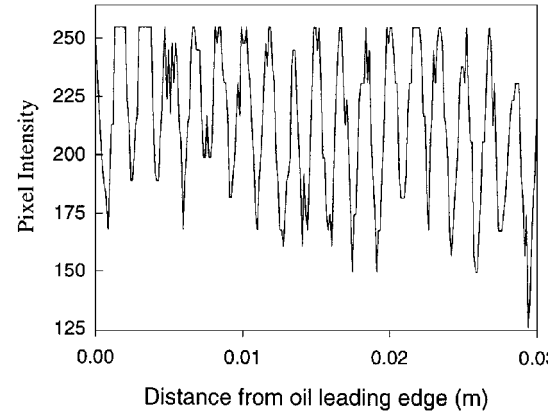

Fig. 5 Pixel intensity variation along a line drawn across the image shown in Fig. 2.

For the Dow silicone oils used, the viscosity obeys the following relation:

$$\mu_0 = \mu_r \exp[c(T_r - T)] \tag{5}$$

where μ_r is a reference viscosity at the reference temperature T_r and c is a known constant. Hence, by measuring the model temperature vs time, the integral involving the viscosity can be evaluated. The streamline spacing variation along each cut through the image can be determined from a separate limiting streamline visualization. Hence, the only unknown in Eq. (4) is the shear stress distribution. An initial guess for $\tau(x)$ can be obtained by applying Eq. (2). Given the initial guess, Eq. (4) is used to obtain updated distributions until the procedure converges.

Results

Computer Simulations

Because there are very few three-dimensional flows for which $\tau(x)$ is accurately known, the initial evaluation of the GISF meter was done using computer simulations. A flowfield was generated with arbitrary variations in the governing parameters such as the shear stress distribution, streamline spacing, and surface temperature variation. With these flowfield characteristics known, an oil film was placed (using the equations of motion for a thin oil film[23]) into this flowfield for a prescribed time and it was deformed to produce a thickness variation. Once this variation was computed, the oil film was hypothetically illuminated with monochromatic light to create a numerical interference pattern corresponding to the prescribed flow conditions. Because these numerically generated data were unrealistically smooth, random noise was added to the interference pattern to produce fringes that more closely resembled those expected from actual testing. Figure 6a is an example of a numerically generated fringe pattern for a flow with $\tau(x) = 15 - 400x + 10{,}000x^2$, and Fig. 6b shows the intensity variation along a cut across this image.

The purpose of the simulation procedure described earlier was to debug the data reduction algorithm and execute several parametric studies before actual testing was begun. An example of the results gathered from this testing procedure is included in Fig. 6c, which plots the shear variation obtained from analysis of the interference pattern shown in Fig. 6a. It can be seen that the GISF data reduction algorithm described earlier can be used to accurately extract the shear distribution in flows with substantial shear variations. Computer simulations, such as those shown in Fig. 6, were performed for a broad range of both two-dimensional and three-dimensional flows with and without variable wall temperature. The three-dimensional flow simulations included a specification of the streamline spacing $n(x)$ as shown in Fig. 4. Accurate results, similar to those shown in Fig. 6, were obtained in all cases.

To further verify the integrity of the method, additional tests were done using independently simulated oil film distributions supplied by NASA Ames Research Center. In these simulations, the oil film equations of motion were solved computationally for an oil film subject to a nonuniform shear distribution on its surface. The resulting oil film shape was then processed through the data reduction algorithm described earlier and the shear distribution determined.

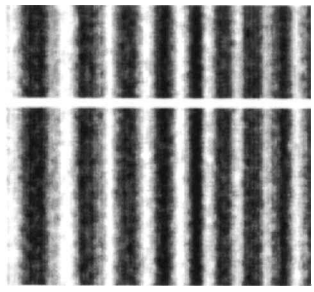

a) Numerically generated fringe pattern for a flow subject to $t = 15 - 400x + 10{,}000x^2$

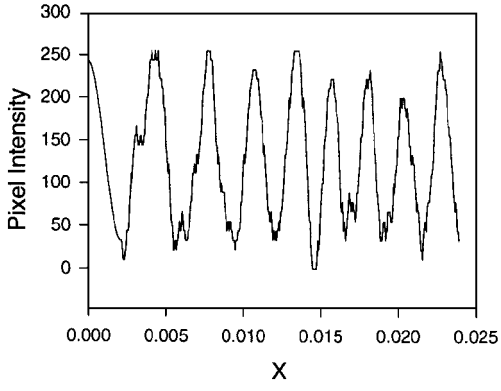

b) Intensity variation along the white line depicted in panel a

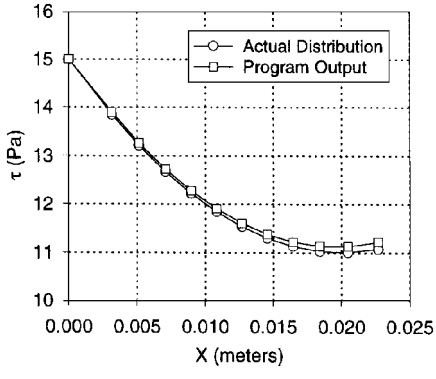

c) Shear stress results

Fig. 6 Sample numerical simulation.

The shear variation computed using Eq. (4) was in excellent agreement with that imposed in the computation, with a discrepancy of less than 1%.

The computer simulations were also used to investigate several parameters that affect the GISF instrument. As mentioned earlier, random noise was added to the signals to create a more realistic image. The magnitude of this noise was varied over a wide range for several different flowfields. In all cases, the algorithm performed well and produced results that matched the flowfield characteristics to within 5%.

The effects of changes in the CCD resolution and image resolution, i.e., pixels per millimeter, were also investigated. As might be expected, an increase in CCD resolution will increase the accuracy of the instrument. With higher resolution, the fringe peaks can be more accurately located, especially in regions where they are very close together. However, the simulations showed that a 512 × 512 CCD array works adequately provided the fringes are spaced sufficiently far apart to be accurately resolved. The other advantage of increased camera resolution is that a larger area may be analyzed in a single image, reducing the time required to obtain skin-friction data over large surfaces.

Flat Plate Experiments

Validation of the GISF meter was performed using the flat plate model described previously. Multiple tests were executed at

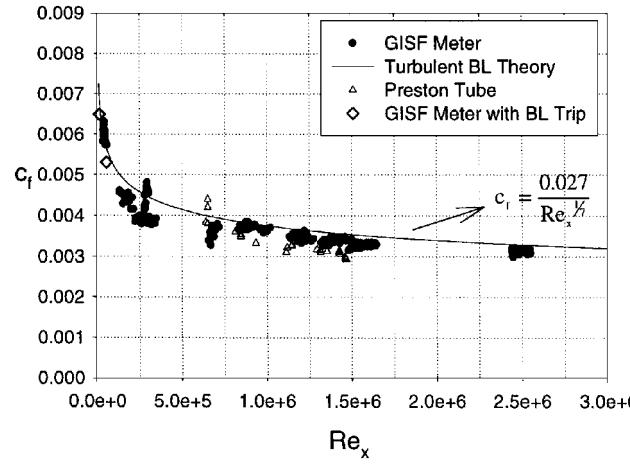

Fig. 7 Summary of flat plate experiments.

Reynolds numbers (based on distance from the leading edge) ranging from 2.5×10^4 to 2.5×10^6. Figure 7 shows the results of those tests along with Preston tube measurements carried out on the same flat plate configuration. The GISF data points represent averaged skin-friction values extracted from 40 wind-tunnel runs. Typically, 12 lines were drawn across each image and the results averaged to determine the shear stress distribution for that particular image. The theoretical curve represents a standard correlation for turbulent boundary layers.[24]

Several things can be observed from Fig. 7. Foremost, the GISF results are in very good agreement with the theoretical result for a turbulent boundary layer and the Preston tube measurements. Over the entire test range, the average deviation between the GISF and theoretical results is 5.93%. The maximum deviation between the GISF and Preston tube measurements is approximately 10.8% with an average deviation of less than 9%. This places the GISF data within the accuracy range of the Preston tube. No Preston tube measurements were performed at Reynolds numbers less than 5×10^5 because the ratio of the tube diameter to the boundary-layer thickness at these measurement locations was greater than 0.1. As stated previously, such situations render the Preston tube measurements unreliable. Additional discussion of the GISF meter's uncertainty is given in a later section.

It can be seen in Fig. 7 that the GISF results follow the turbulent prediction to extremely small Reynolds numbers where one would expect laminar flow. Initially it was assumed that the GISF results were in error in this region. However, further exploration yielded evidence that supported the presence of a turbulent boundary layer at these conditions. First, as noted in the description of the test facility, at its lowest operating velocity the wind tunnel used for the present experiments has an exceptionally high freestream turbulence level (≈6%). It is well documented in the literature (cf. Refs. 25 and 26) that high freestream turbulence levels can lead to early transition. Additionally, the flat plate used in the present experiments had a sharp leading edge, increasing its receptivity to disturbances. Finally, a surface flow visualization revealed the presence of a separation bubble on the top of the flat plate near the leading edge. Hence, all these factors help support the argument that the boundary layer in the present experiments undergoes transition very near its inception and that the shear measured by the GISF instrument at the lower Reynolds numbers is an accurate representation of the flow.

To further support this theory, a trip wire was placed near the leading edge of the flat plate, and two of the lower Reynolds number cases were repeated. Results from the measurements with the trip wire in place are also shown in Fig. 7. The results obtained with the trip wire are nearly identical to those without the wire and help support the argument that the boundary layer becomes turbulent very near its inception. Detailed measurements of the flat plate boundary-layer profile would be useful for conclusively proving this conclusion. However, because the boundary layer is extremely thin in this region, such measurements are difficult to perform.

To determine the approximate origin of the boundary layer, an oil film was applied at the front of the plate with its leading edge

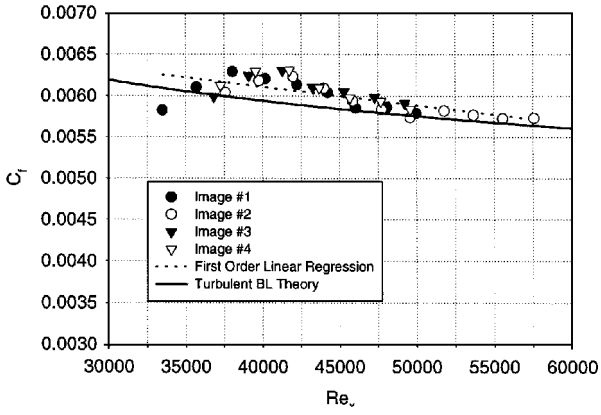

Fig. 8 Spatial shear variation for two runs with different oil leading-edge locations.

oriented to intersect the plate leading edge at approximately 45 deg. By applying the oil along a diagonal, it was possible to determine the location on either side of which the oil flowed in opposite directions. Based on these results, the flow attachment point was determined to be approximately 12 mm downstream of the plate edge. This point was taken as the origin for the boundary layer.

Figure 8 illustrates the GISF instrument's ability to measure the shear variation in the streamwise direction. This figure plots the shear variation vs distance from the origin of the turbulent boundary layer for four sets of runs. The experimental data shown in Fig. 8 represent the ensemble-averaged shear distribution obtained from 12 cuts per image. The four data sets were collected for oil films with their leading edges located approximately 2.5 cm from the boundary-layer origin. Measurements were taken close to the origin because the shear variation in this region is significant. Overall, there is very good agreement between the experimental and theoretical shear values. The maximum deviation along the first-order regression line is less than 3%, and the maximum deviation of any data point on the plot is less than 8%, indicating that the present GISF instrument can accurately measure the shear variation in the streamwise direction. These results also help support the argument that the boundary layer becomes turbulent very near its inception.

Overall, even though there is some uncertainty in the nature of the flat plate boundary layer at the lower numbers, the higher Reynolds number data points clearly show that the GISF instrument can accurately measure the wall shear stress with accuracies on the order of $\pm 8\%$. It is believed that, with further refinements to both the data reduction algorithm and the experimental procedure, the accuracy of the instrument can be further improved. An error analysis of the simplified Eq. (3) indicates that uncertainties on the order of $\pm 5\%$ can be obtained using relatively standard instrumentation. Through more accurate measures to record the oil temperature and the use of a high-resolution CCD camera, even better uncertainty levels may be attainable. Additional discussion of the factors influencing the instrument's uncertainty appears in the following section.

Parametric Investigations

Several parametric studies were conducted to evaluate the performance of the GISF meter. The theory in Eqs. (1–5) assumes that the shear does not vary with time. However, it is known that such variations occur during the wind-tunnel startup and shutdown processes. Thus, both these processes were examined to determine their influence on the GISF results. All of this testing was executed using the flat plate model.

Shutdown

The first investigation was to study the effect of wind-tunnel shutdown. A series of nine wind-tunnel runs were conducted (three each at three different Reynolds numbers). Three images were taken at different times during each run. The first image of the oil film was grabbed immediately before shutdown. The second was grabbed 10 s after the onset of shutdown and the final image 80 s after the onset of shutdown. The time used for computation in all cases was the time up to the onset of shutdown. In all cases, the shear values

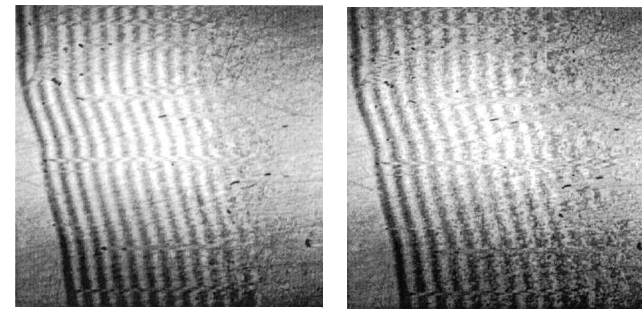

Just before wind-tunnel shutdown **Two minutes after shutdown**

Fig. 9 Interference patterns taken.

obtained from the images acquired just after shutdown tended to be slightly larger than those obtained just before shutdown. This trend was expected because the velocity in the test section is still relatively high during the first 10 s after shutdown. The fringes are still deforming during this period, and the time used for computation is held constant for the two images. This results in a computed shear that is higher than that from the first image.

The data extracted from the third set of images tended to be more erratic. This is possibly caused by the degradation of the fringes with time. An example of such an image is shown in Fig. 9. The degradation time of the fringes was observed to be a function of dust contamination, temperature, and relative humidity. Nonetheless, analysis of all the shutdown results showed that, regardless of when the images were taken, the deviation between the measured and theoretical shear was always less than 10% and the maximum deviation between any two experimental readings was 17%. Hence, these results show that acceptable accuracy can be obtained by acquiring the oil interference pattern after the test run is complete. However, if optical access is available, the preferred approach is to acquire the image just before shutdown.

Startup

Analogous to the shutdown tests, a series of runs was performed to examine the influence of the wind-tunnel startup time. This was done by varying the amount of time the tunnel took to reach operating conditions. It was found that when the startup time is a high percentage of the total run time, lower values for the shear stress are computed. In general, the percent error in the measured wall shear was equal to the fraction of the total run time occupied by the startup process, e.g., if the startup time was 30% of the total time, the measured shear was 70% of the actual value. This effect is considerably more important than the shutdown process and emphasizes the importance of keeping the startup time much less than the total run time. In some instances, however, the startup (or shutdown) times cannot be reduced to a negligible percentage of the total run time. To account for this, the freestream pressure can be monitored during the run and integrated.[19,27] This may be used to adjust the wind-tunnel run time to produce a better estimate of the skin-friction values.

Related tests were performed in which the freestream velocity was changed during a particular run. These tests were conducted by starting the wind tunnel at one particular velocity for a prescribed length of time and then increasing the speed to a new value for the duration of the run. The analysis procedure applied to images taken at the end of the test produced shear stress values representing the average shear stress acting on the oil surface during the run.

Run Time

An investigation of the effect of the overall wind-tunnel run time was also conducted. Provided the run time met the criterion of being much greater than the wind-tunnel startup time, runs of considerably different duration gave essentially the same results. However, because a direct relationship exists between the run time and the computed shear stress, measurement of the run time is critical. Because there is some uncertainty in deciding when the run timer should be started, the error introduced by this effect is minimized by an extended run time. It is also noted that a longer run time

produced fringes over a larger area. For the present tests, fringes were consistently obtained over a rectangular area of approximately 6.3×5.1 cm.

Oil Viscosity

In another parametric study, the oil viscosity was varied over a series of wind-tunnel runs while all other test conditions were maintained. As the oil viscosity was lowered, the oil film deformed more rapidly, requiring shorter run times. For relatively low viscosities, the run time had to be very short in relation to the wind-tunnel startup time. As discussed in the preceding section, this added some uncertainty to the calculations. Regardless of the oil viscosity, as long as the run time was much greater than the startup time, results were independent of oil viscosity. However, it was observed that the lower viscosity oils tended to be more sensitive to model surface imperfections and contaminants such as dust. As mentioned earlier, the degradation of the oil film after shutdown is governed by several factors including the oil viscosity. In performing the oil viscosity study, it was observed that fringes in higher viscosity oils degraded at a slower rate than lower viscosity oils and retained the fringe pattern for a longer period.

Error Analysis

The computer simulation of the equations of motion for the oil film and the data reduction algorithm were used to perform an error analysis of the GISF technique. A study of the errors resulting from uncertainties in the measured quantities used in the analysis revealed that uncertainties in oil viscosity and locating the oil film leading edge (OLE) location produce the greatest effect in the final estimate of the shear stress values. Depending on testing conditions, a 1% error in the value of the oil viscosity can produce a 4% deviation in the estimated shear stress. Because the oil viscosity is determined from the known properties of the oil and its temperature, the model surface temperature must be measured with an uncertainty of less than 1°C to minimize the error in the final result.

The accuracy in locating the OLE is limited by the resolution of the image. Its effect on the final results is also dependent on the number of pixels between fringes in the image. Also, as the distance from the OLE increases, the uncertainty in locating the OLE becomes significantly less important. This is revealed in the erratic nature of the shear stress values estimated at the first two or three fringes. Because the error created by this effect depends on the image resolution, it may be necessary (in some instances) to discard the data obtained from the first few fringes in the image to ensure the accuracy of the final results. A detailed discussion of the effects of the uncertainties in additional parameters is given in Ref. 27.

Future Work

More complete validation of the GISF instrument is planned or is currently under way. Future testing will focus on geometries for which the surface shear stress varies more substantially in the flow direction and for flows with variable wall temperatures. Some potential configurations planned for investigation include flow over a cylinder, flow above a rotating disk, and a stagnating jet flow. These flows were selected because analytical and/or experimental results exist that can be used for validation of the results. Also, cylinder base flows and flow over a backward facing step may also be considered for validation of the GISF instrument in complex flows. However, these geometries have limited theoretical predictions, and there is a lack of accurate data or methods with which to compare the GISF results. Also, tests in supersonic tunnels would be extremely beneficial to further validate the instrument. Moreover, the startup and shutdown processes in supersonic tunnels are substantially different than those in low-speed tunnels; additional study of these processes in supersonic flows would better clarify their impact.

Conclusions

The GISF meter provides an improved method for measuring skin friction. Accurate results have been recorded during testing on a flat plate model at a wide range of Reynolds numbers. Several parametric studies showed that the fraction of the total wind-tunnel test occupied by tunnel startup had a significant effect on the measured results. Although startup was found to be a possible source of error, testing showed that wind-tunnel shutdown had only a minor effect on the results. The duration of the wind-tunnel run and the oil film viscosity had little effect on the computed shear stress results provided the wind-tunnel run time was significantly larger than the startup time. The GISF meter described herein provides numerous advantages over other shear measurement devices. The instrument is inexpensive to assemble, and the equipment and data analysis method are relatively simple to implement. The instrument has been validated with experiments in two-dimensional flows. However, with the theory presented in the present paper, the technique shows promise in providing global shear data in fully three-dimensional flows with nonuniform wall temperatures. The instrument is also insensitive to vibration, dust particles, and surface waves and requires no calibration. These features will make the GISF meter invaluable for analysis of a wide variety of flows and for assembling data for computational fluid dynamics validation. However, further testing in complex flows (currently in progress) is needed to completely validate the instrument.

Acknowledgments

The authors would like to thank the Louisiana Education Quality Support Fund through LaSPACE under agreement NASA/LSU (1991–96)-01 and NASA Grant NGT-40039 for support of this project. The authors would like to thank Jonathan Naughton and James Brown at NASA Ames Research Center for providing the computed oil film patterns. The authors would also like to thank Stephen Guillot for his assistance in executing the experiments.

References

[1]Winter, K. G., "An Outline of the Techniques Available for the Measurement of Skin Friction in Turbulent Boundary Layers," *Progress in Aerospace Science*, Vol. 18, 1977, pp. 1–57.

[2]Tanner, L. H., and Blows, L. G., "A Study of the Motion of Oil Films on Surfaces in Air Flow, with Application to the Measurement of Skin Friction," *Journal of Physics E: Scientific Instruments*, Vol. 9, No. 3, 1975, pp. 194–202.

[3]Tanner, L. H., "A Skin Friction Meter, Using the Viscosity Balance Principle, Suitable for Use with Flat or Curved Metal Surfaces," *Journal of Physics E: Scientific Instruments*, Vol. 10, March 1977, pp. 278–284.

[4]Tanner, L. H., and Kulkarni, V. G., "The Viscosity Balance Method of Skin Friction Measurement: Further Developments Including Applications to Three-Dimensional Flow," *Journal of Physics E: Scientific Instruments*, Vol. 9, No. 12, 1976, pp. 1114–1121.

[5]Monson, D. J., and Higuchi, H., "Skin Friction Measurements by a Dual-Laser-Beam Interferometer Technique," *AIAA Journal*, Vol. 19, No. 6, 1981, pp. 739–744.

[6]Murphy, J. D., and Westphal, R. V., "The Laser-Interferometer Skin-Friction Meter—A Numerical and Experimental Study," *Proceedings of the Third Symposium on Numerical and Physical Aspects of Aerodynamic Flows*, 1985 (Paper 7-1).

[7]Monson, D. J., Driver, D. M., and Szodruch, J., "Application of a Laser Interferometer Skin-Friction Meter in Complex Flows," *Proceedings of the International Congress on Instrumentation in Aerospace Simulation Facilities*, Inst. of Electrical and Electronics Engineers, 1981, pp. 232–243 (81CH1712-9).

[8]Monson, D. J., "A Nonintrusive Laser Interferometer Method for Measurement of Skin Friction," *Experiments in Fluids*, Vol. 1, No. 1, 1983, pp. 15–22.

[9]Kim, K.-S., and Settles, G. S., "Skin-Friction Measurements by Laser Interferometry," *A Survey of Measurements and Measurement Techniques in Rapidly Distorted Compressible Boundary Layers*, edited by H. H. Fernholz, A. J. Smits, and J. P. Dussauge, AGARDograph 315, 1988, pp. 4.1–4.8.

[10]Kim, K.-S., and Settles, G. S., "Skin Friction Measurements by Laser Interferometry in Swept Shock/Boundary-Layer Interactions," *AIAA Journal*, Vol. 28, No. 1, 1990, pp. 133–139.

[11]Garrison, T. J., Settles, G. S., Narayanswami, N., and Knight, D., "Laser Interferometer Skin-Friction Measurements of Crossing-Shock Wave/Turbulent Boundary-Layer Interactions," *AIAA Journal*, Vol. 32, No. 6, 1994, pp. 1234–1241.

[12]Wideman, J. K., Brown, J. L., Miles, J. B., and Özcan, O., "Skin-Friction Measurements in Three-Dimensional, Supersonic Shock-Wave/Boundary-Layer Interaction," *AIAA Journal*, Vol. 33, No. 5, 1995, pp. 805–811.

[13]Garrison, T. J., Manceau, E., and Nikitopoulos, D. E., "Skin Friction Measurements in a Gas-Liquid Pipe Flow via Optical Interferometry," *Proceedings of the 1996 ASME Symposium on Cavitation and Gas-Liquid Flows in Machinery and Devices*, Vol. 2, American Society of Mechanical Engineers, 1996.

[14] Kornilov, V. I., Pavlov, A. A., and Shpak, S. I., "On the Techniques of Skin Friction Measurement Using Optical Method," International Conf. on the Methods of Aerophysical Research—ICMAR '92, Novosibirsk, Russia, 1992.

[15] Kornilov, V. I., Pavlov, A. A., and Shpak, S. I., "On the Techniques of Skin Friction Measurement Using Optical Method in Supersonic Flow," *Siberian-Physical Technical Journal*, Vol. 6, 1991, pp. 47–52.

[16] Maksimov, A. I., Pavlov, A. A., and Shevchenko, A. M., "Development of the Optical Skin Friction Measurement Technique for Supersonic Gradient Flows," International Conf. on the Methods of Aerophysical Research—ICMAR '94, Novosibirsk, Russia, 1994.

[17] Siller, H. A., "An Optical Method of Measuring Wall Shear Stress Using Oil Film Interferometry and Image Processing Techniques," Ph.D. Dissertation, Mechanical Engineering Dept., Univ. of Cambridge, Cambridge, England, UK, 1991.

[18] Siller, H. A., Perkins, R. J., and Janke, G., "Image Analysis of Oil Film Interferometry—A Method of Measuring Wall Shear Stress Distributions," *Flow Visualization and Image Analysis*, Kluwer Academic, Norwell, MA, 1993, pp. 71–80.

[19] Monson, D. J., Mateer, G. G., and Menter, F. R., "Boundary Layer Transition and Global Skin Friction Measurement with an Oil-Fringe Imaging Technique," Society of Automotive Engineers, Aerotech '93, SAE Paper 932550, Sept. 1993.

[20] Mateer, G., Monson, D., and Menter, F., "Skin-Friction Measurements and Calculations on a Lifting Airfoil," *AIAA Journal*, Vol. 34, No. 2, 1996, pp. 231–236.

[21] Head, M. R., and Ram, V. V., "Simplified Presentation of Preston Tube Calibration," *Aeronautics Quarterly*, Vol. 22, 1971, pp. 295–300.

[22] Goldstein, R. J., *Fluid Mechanics Measurements*, 2nd ed., Taylor and Francis, Washington, DC, 1996, pp. 582–586.

[23] Squire, L. C., *Motion of a Thin Oil Sheet Using the Boundary Layer on a Body*, AGARDograph 70, 1962, pp. 7–23.

[24] White, F. M., *Viscous Fluid Flow*, 2nd ed., McGraw–Hill, New York, 1991, Chap. 6.

[25] Van Driest, E. R., and Blumer, C. B., "Boundary Layer Transition: Freestream Turbulence and Pressure Gradient Effects," *AIAA Journal*, Vol. 1, No. 6, 1963, pp. 1303–1306.

[26] Reshotko, E., "Boundary Layer Instability, Transition, and Control," AIAA Paper 94-0001, Jan. 1994.

[27] Zilliac, G. G., "Further Developments of the Fringe-Imaging Skin Friction Technique," NASA TM 110425, Dec. 1996.

G. Laufer
Associate Editor